ACCEPTED MANUSCRIPT

Final published version of this article: Ceramic International, Volume 49 (2023), 24312-24321

Available online: 5 December 2022
DOI: https://doi.org/10.1016/j.ceramint.2022.12.013

Studying stearic acid interaction with ZnO/SiO_2 nanoparticles with tailored morphology and surface features: a benchmark for better designing efficient ZnO-based curing activators.

Silvia Mostoni [a], Paola Milana [a], Massimiliano D'Arienzo [a], Sandra Dirè [b], Emanuela Callone [b], Cinzia Cepek [c], Silvia Rubini [c], Aysha Farooq [c] Carmen Canevali [a], Barbara Di Credico [a] and Roberto Scotti [a,d]*

[a] Department of Materials Science, INSTM, University of Milano-Bicocca, Via R. Cozzi 55, 20125 Milano, Italy;

[b] Department of Industrial Engineering (DII), University of Trento, Via Sommarive 9, 38123, Trento, Italy;

[c] Istituto Officina dei Materiali-CNR Laboratorio TASC, Strada Statale 14, km 163.4, I-34012 Trieste, Italy

[d] Istituto di Fotonica e Nanotecnologie-CNR, via alla Cascata, 56/C, 38100, Povo, Trento, Italy

KEYWORDS: Zinc oxide; Vulcanization; Activator; Stearic acid; surface interaction.

ABSTRACT

The interaction between activators (ZnO) and co-activators (stearic acid, SA) represents a key step in the vulcanization process, to generate Zn(II) intermediate complexes that enhance the reaction kinetic and promote the shortening of sulfur bridges, leading to highly cross-linked materials. To understand the influence of the structural, morphological and surface properties of ZnO in the reactivity with SA, in this work, pure ZnO nanoparticles (NPs) and ZnO NPs anchored on SiO_2 (ZnO/SiO_2) were prepared through soft chemistry techniques. Tailoring of morphology and surface features was accomplished through a fine control of the synthetic parameters, as demonstrated by the careful characterization of the activators. Then, the interaction of pure ZnO and ZnO/SiO_2 activators with SA in the absence of rubber was investigated by using Differential Scanning Calorimetry (DSC). The occurrence of Zn(II)-SA complexes with different thermal stability and structural properties was assessed by a comprehensive thermogravimetric and spectroscopic survey. The generation and the chemical structure of these specific vulcanization intermediates was related to the peculiar characteristics of the ZnO/SiO_2 systems and, in turn, to their ability in imparting faster kinetics and higher curing efficiency to isoprene rubber nanocomposites, compared to bare ZnO.

These results, besides proposing a valid benchmark for achieving further insights on the interaction of stearic acid with activators, pave the way to provide specific protocols for a better design and implementation of ZnO-based materials able to effectively enhance the rubber vulcanization process, with significant economic and environmental advantages.

INTRODUCTION

The performances of rubber materials, used in different applications as tires, strongly depend on the sulfur vulcanization process, as it enables the formation of sulfur-based chemical cross-links between the elastomer chains that contribute to the reinforcement of the organic matrix [1-5]. To facilitate the sulfur interaction with the elastomer, shorten the vulcanization time and lower the energy consumption, curing agents are employed [1-11]. These are: i) organic accelerators such as N-cyclohexyl-2-benzothiazole sulfenamide (CBS) and tetramethylthiuram disulfide (TMTD) [3], ii) inorganic activators, like ZnO [6-10] and iii) co-activators as fatty acids (mainly stearic acid, SA) [11] which, in conjunction with activators ensure the formation of active Zn(II) centers [10]. More in depth, it is widely recognized that in the first reaction steps, ZnO interacts with SA to create highly reactive Zn(II)-SA adducts, generally in the form of zinc stearate, which then react with both accelerator and sulfur, providing Zn complexes containing poly-sulfidic ligands, which represent the active sulfurating agents [10-12]. These units are believed to drive the subsequent reactions with the polymer chains and the formation of poly-sulfidic pendant cross-link intermediates, that progressively shorten through decomposition and rearrangement reactions endorsed by Zn(II) sites, delivering highly cross-linked products [10-12].

Thus, the generation of zinc centers at the beginning of the reaction represents a critical step as it determines both the reaction kinetic and the resulting properties of the cross-linked network [13]. In fact, several studies have demonstrated that the use of both ZnO and SA is crucial not only for chemical cross-linking of the rubber molecules, but also for controlling structural polymer network inhomogeneity in the sulfur cross-linked rubber [14-19]. Combining *in situ* time-resolved zinc K-edge X-ray absorption fine structure spectroscopy, *in-situ* time-resolved Fourier-transform infrared spectroscopy (FTIR), and density functional theory calculations, Ikeda and co-workers proved the generation of a new dinuclear type bridging bidentate zinc/stearate complex composed of $[Zn_2(\mu\text{-}O_2CC_{17}H_{35})_2]^{2+}\cdot 4X$, where X is hydroxyl group, water and/or rubber segment [14-16]. This peculiar species was found to accelerate the hydrolysis reaction of CBS, the insertion reaction of sulfur atoms along with the generation of abundant di-sulfidic linkages in the rubber compounds [15].

In the last decade, we have pursued the study of the vulcanization process by exploring the influence of Zn(II) centers dispersion and availability on the curing efficiency of isoprene rubber (IR) [10, 20-22]. In detail, an innovative activator based on ZnO nanoparticles (NPs) directly grown on the silica surface (ZnO/SiO_2), that behaves at the same time as a vulcanization activator and a reinforcing filler, has been developed by exploiting soft-chemistry methods [20, 21]. Successively, the investigation has been also extended to Zn(II) single sites anchored on the surface of SiO_2 NPs, through surface functionalization with amino silane followed by the coordination of Zn(II) centers to the amino groups [22]. These materials having double functionalities demonstrated higher efficiency in the curing process compared to microcrystalline ZnO, conventionally employed as an activator for industrial rubber vulcanization, with a relevant impact both on the reaction kinetics and on the dynamic mechanical properties of the vulcanized composites, as well as reducing the whole amount of employed ZnO [20-22]. The results have been ascribed to the unique characteristics of the activators, which supply Zn(II) catalytic sites readily accessible to the curing agents, possibly endowing a reaction pathway where the formation of the highly reactive zinc/stearate complexes retrieved by Ikeda et al. [14-16] boosts the curing process.

Although the above-cited experimental evidences remarkably contributed to a better understanding and control of the rubber vulcanization, it remains almost unexplored if and how the structural, morphological and surface characteristics of the novel Zn-based activators effectively influence their reactivity with SA, which represents a determinant step for the process efficiency. Try to face with these challenges, the present investigation focuses on a comprehensive comparison between the properties and the reactivity with SA of pure ZnO and ZnO/SiO_2 systems with different structural, morphological and surface features. In a wider perspective, this study aims also at unveiling how the anchoring of ZnO NPs with controlled morphological properties and its synergy with SiO_2 support may influence the surface interaction with carboxylic species as SA.

Besides a careful characterization of the activators, an extensive spectroscopic survey carried out by X-ray Photoelectron Spectroscopy (XPS) revealed the occurrence of various inequivalent zinc and oxo-hydroxo species at the surface of ZnO NPs, possibly impacting on the Zn(II) reactivity and complexation.

The interaction between the different ZnO/SiO_2 activators with SA, in the absence of rubber, was studied by a combination of several techniques: Differential Scanning Calorimetry (DSC) and ThermoGravimetric Analysis (TGA), to monitor and highlight different phase transitions, thermal events and reaction products stability; FTIR and solid-state nuclear magnetic resonance (NMR) spectroscopies to gain structural information on the SA coordination at the Zn sites. Through this novel methodological approach, interesting correlations have been drawn among the morphological and interfacial features of ZnO/SiO_2 systems, the thermal events observed in DSC and the generation of different Zn(II)-SA complexes, as revealed by FTIR and NMR. Finally, in order to demonstrate how these characteristics affect the vulcanization process, the proposed ZnO/SiO_2 materials were tested as activators in the curing reaction of isoprene rubber (IR) nanocomposites (NCs).

The results highlighted that morphology and surface control of the ZnO activators enable not only a peculiar reactivity with stearic acid, but remarkably impact also on the vulcanization performance delivered to the resulting rubber nanocomposites, providing specific hints for a better design and implementation of efficient ZnO-based activators.

EXPERIMENTAL

Materials. Zinc acetate dihydrate (≥ 98%), sodium hydroxide pellets (NaOH, ≥ 98%), ammonium hydroxide solution (NH_4OH, 25%), tetraethylorthosilicate (TEOS) and SA (98%) were purchased from Merck Life Science; absolute ethanol (EtOH) and water (for HPLC instrument) were purchased from VWR International. For rubber NCs: cis-1,4-polyisoprene rubber (IR) was purchased from Nizhnekamskneftechim Expor; bis(3-triethoxysilylpropyl) disulfide (TESPD) from Aldrich; antioxidant N-(1,3-dimethylbutyl)-N'-phenyl-p-phenylenediamine (6PPD), Santoflex-6PPD from Flexsys. The curing agents were purchased as follows: SA (Stearina TP8) from Undesa; N-cyclohexyl-2-benzothiazole sulphenamide (CBS), Vulkacit CZ/X from Lanxess; sulfur Creso from Redball Superfine; ZnO (wurtzite, specific sur-face area 5 m^2g^{-1}) from Zincol Ossidi.

Synthesis of ZnO/SiO₂. ZnO/SiO_2 NPs were prepared by a two-step procedure, developed by modifying an established previously reported approach [20]. The method is relatively fast, and it generally enables the control of both ZnO NPs loading and distribution on the silica surface.

In the first step, SiO_2 particles with spherical shape, nanometric size (d = 60-70 ± 5 nm) and BET specific surface area SSA_{BET} = 66.6 ± 0.8 m^2g^{-1}, were prepared according to a conventional Stöber method [23, 24]. ZnO NPs were then grown onto the silica surface exploiting the method reported in [20]. Briefly, $Zn(CH_3COO)_2 \cdot 2H_2O$ (0.337 g) and NaOH (0.28 g) were dissolved in 70 mL of EtOH or water at 65°C. Then, 1.0 g of SiO_2 NPs was then poured into the former zincate solution and kept under stirring at 65 °C for 20 min, to promote the generation of ZnO NPs by hydrolysis and condensation on the silica surface. The product was filtered, successively washed with EtOH (or water, respectively) and dried in air at room temperature (RT). The nominal composition of the catalyst corresponds to 12 wt. % of ZnO on SiO_2. The samples obtained from EtOH and H_2O as solvents were labelled as ZnO/SiO_2_EtOH and ZnO/SiO_2_H_2O, respectively. As reference material, bare ZnO NPs were synthesized with the same protocol in water without silica addition and labelled simply as ZnO.

Structural, morphological and surface characterization of ZnO/SiO₂ activators. The loading of Zn in the samples was determined by Inductively Coupled Plasma Optical Emission Spectrometry (ICP-OES), using a PerkinElmer OPTIMA7000 DV spectrophotometer. Specimens for the analysis were prepared by dissolving 0.20 g of powdered samples in a Teflon beaker with 4.0 mL of HNO_3, 3.0 mL of HCl and 1.0 mL of HF. The dispersion was diluted with 12 mL of milli-Q H_2O and then further diluted to 1:100.

Powder X-ray diffraction (PXRD) patterns were collected with a Rigaku Miniflex 600 diffractometer (Cu Kα radiation) in the 2θ range 10-80° (2θ step 0.020°, 1 ° min^{-1} scan rate).

High-resolution transmission electron microscopy (HRTEM) was performed using a JEOL JEM-2100 Plus apparatus operating at 200 kV and equipped with an 8-megapixel Gatan RioTM complementary metal-oxide-semiconductor (CMOS) camera. A 5 μL drop of ethanol powder samples suspension was deposited onto a carbon coated copper mesh grid for TEM investigation.

Reflectance UV–vis analysis (range 400–200 nm) was performed by a UV Lambda 900 Perkin Elmer spectrometer on powdered samples to determine the absorption edge energy of ZnO. The absorption onset can be obtained by plotting F(R) vs. energy according to the Kubelka Munk equation [25] and the band gap energy (E_g) derived from the intercept point of the tangents to the curve at the slope and at the minimum.

Structural information on ZnO/SiO_2 systems was achieved by solid state NMR. Experiments were carried out with a Bruker 400WB spectrometer operating at a proton frequency of 400.13 MHz. Magic Angle Spinning (MAS) NMR spectra were acquired with cross polarization (CP) sequence under the following conditions: ^{29}Si frequency: 79.48MHz, contact time 5 ms, decoupling length 6.3 μs, recycle delay: 10 s, 5 k scans. Samples were packed in 4 mm zirconia rotors, which were spun at 6.5 kHz under air flow. Q8M8 was used as external secondary reference. According to the common ^{29}Si NMR notation, the Si species are labelled Q^n, where Q represents SiO_4 structural units, and n is the number of bridging oxygens.

The surface chemical composition of the ZnO/SiO_2 powders was investigated by XPS. The measurements were performed on the as-prepared powder samples, fixing them on the sample holder using carbon tape. The XPS spectra were acquired in ultrahigh vacuo (base pressure: $\sim 5 \times 10^{-10}$ mbar) at RT in normal emission geometry using a conventional Mg X-ray source (hν = 1253.6 eV) and a hemispherical electron energy analyzer (120 mm by PSP: total energy resolution ~ 0.8 eV, standard deviation ± 0.2 eV). Due to charging effects, all binding energies (BE) were calibrated by fixing the C 1s BE of atmospheric contamination at 284.8 eV. Survey scans were obtained in the 0–1100 eV range, while detailed scans were recorded in the BE regions corresponding to O 1s, C 1s, Si 2p, and Zn 2p levels. The O 1*s* and Zn 2$p_{3/2}$ XPS spectra were reproduced by fitting the experimental data using a Shirley background and several Doniach-Sunjich components, corresponding to different oxidation states and chemical environments.

Study of the SA interaction with ZnO/SiO₂ samples. The interaction of SA with ZnO/SiO_2 samples was investigated by DSC, which allows to monitor different phase transitions, thermal events and to earn information about the possible generation/evolution of reaction products. Components (SA and ZnO/SiO_2, 1:1 molar ratio) were mixed in a mortar to obtain a homogeneous powder. Samples (5-8 mg) were weighted on a microbalance, compressed to ensure good thermal contact, and enclosed in a 40 μL aluminum pan with pierced lid. To simulate the conditions of the vulcanization reaction, mixtures were heated in a DSC-1 system (Mettler Toledo). Experiments were performed using a three steps temperature ramp: i) temperature was increased starting from 30 to 200 °C with a heating rate of 5 °C min^{-1}; ii) samples were brought back to 30°C (heating rate -10 °C min^{-1}); iii) a final heating step to 200 °C (heating rate 5 °C min^{-1}) was lastly performed. All the experiments were carried out under nitrogen flow (80 mL min^{-1}).

The samples recovered from DSC and thus reacted with SA were analyzed by TGA to inspect the thermal stability of the reaction products, also in comparison to that of pure SA and bare crystalline zinc stearate. Experiments were performed using a TGA/DCS1 STARe SYSTEM in the temperature range 30-700 °C, constant air flow (50 mL min^{-1}), heating rate of 10 °C min^{-1}; an isothermal step at 200 °C (15 min) was used to complete the weight loss due to physisorbed solvent molecules and water.

To gain structural information on the SA coordination at the Zn centers, ZnO/SiO_2_EtOH and ZnO/SiO_2_H_2O powders after DSC were initially analyzed by FTIR in Attenuated Total Reflectance mode (ATR-FTIR with a monolithic diamond crystal). Spectra were acquired using a

Perkin Elmer Spectrum 100 instrument in the region 650–4000 cm^{-1} and with a resolution of 2 cm^{-1} (32 scans).

More detailed information on the local binding modes of carboxylic groups of SA at the interface of ZnO/SiO_2 samples were achieved by ^{13}C solid state NMR experiments, which were recorded with cross polarization pulse sequence at spinning rate of 6.5 kHz under the following conditions: ^{13}C frequency 100.48 MHz, contact time 2 ms, decoupling length 5.9 µs, recycle delay: 3 s, 4k scans. Adamantane was used as external secondary reference.

Preparation of silica/IR nanocomposites. The performance of ZnO/SiO_2 curing activators for the vulcanization of rubber-based materials were preliminary tested by preparing silica/IR NCs. The ingredients were mixed in a Brabender Plasti-Corder lab station internal mixer (65 mL mixing chamber, 0.6 filling factor, 60 rpm rotor speed). First, IR was masticated into the mixing chamber at 145 °C and a suitable amount of ZnO/SiO_2 and bare SiO_2 were added, in order to have 1.85 parts per hundred (phr) of ZnO and 40 phr of SiO_2 filler, respectively, along with TESPD compatibilizing agent (3.2 phr). After 3 min of mixing, the antioxidant 6-PPD (2.0 phr) and SA (2.0 phr) were added and further mixed for 1 min. The composites were then reloaded into the mixing chamber at T = 90 °C and CBS (3.0 phr) and S_8 (1.6 phr) were added (2 min of mixing). Finally, the NCs were mixed in a two-rolling mill at 50 °C for 3 min, to improve their homogeneity. Reference IR NCs were prepared by using bare SiO_2 filler (40 phr) and microcrystalline ZnO curing activator (1.85 phr). The vulcanization reaction was performed by using a Rubber Process Analyzer (RPA2000, Alpha Technologies). The vulcanization curves were registered at 170 °C and 100 bar (frequency = 1.670 Hz, angle = 6.980 °) for a vulcanization time = 5 min, by measuring the torque requested to keep the rotor at a constant rate over the time to evaluate the viscosity.

RESULTS AND DISCUSSION

Structural and morphological characterization of ZnO/SiO_2 activators.

The ZnO amount in the prepared activators was assessed by ICP-OES analysis and resulted 8.5±0.1 wt. % and 8.9±0.1 wt. % for ZnO/SiO_2_EtOH and ZnO/SiO_2_H_2O, respectively, i.e. values merely similar to the nominal ones (~ 12 wt. %), with a reaction yield of about 70 % in both cases.

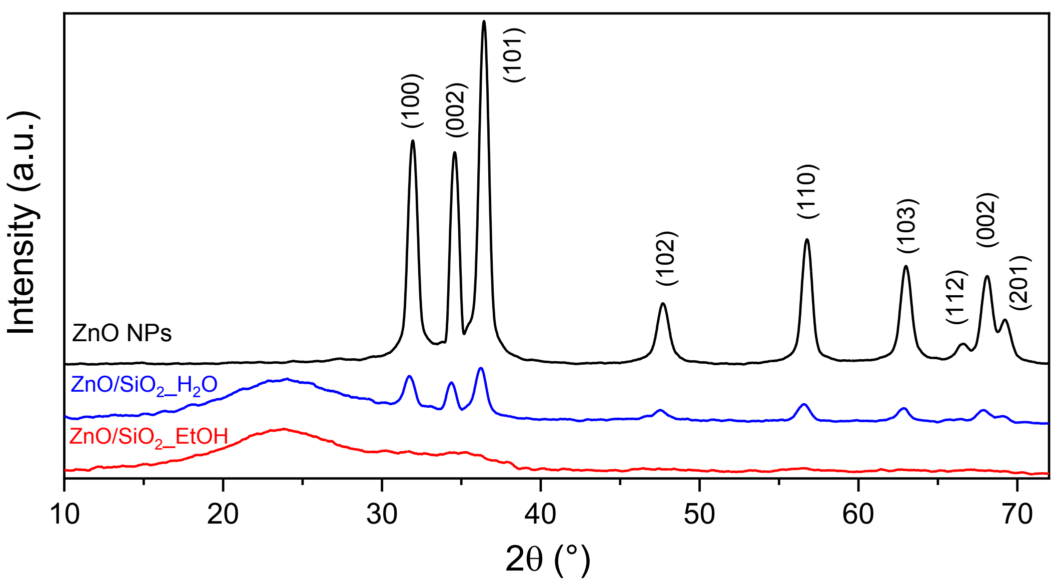

Figure 1. Powder XRD patterns of bare ZnO NPs (black line), ZnO/SiO_2_EtOH (red line) and ZnO/SiO_2_H_2O (blue line) systems. All the indexed peaks are matched with the planes of the ZnO hexagonal wurtzite structure (JCPDS no.36-1451).

The structural features of ZnO and ZnO/SiO_2 powders were investigated by PXRD (Figure 1). Besides the broad band at ~ 22 ° connected to the presence of amorphous SiO_2 NPs, the typical reflections of hexagonal wurtzite ZnO crystal phase (JCPDS no.36-1451) are clearly detectable for ZnO and ZnO/SiO_2_H_2O NPs, while they appear just roughly sketched in the sample prepared in EtOH. The sharp peaks observed for pure ZnO and, though less intense, in ZnO/SiO_2_H_2O suggest a higher crystallization degree and an increased average size of the ZnO NPs compared to the ZnO/SiO_2_EtOH system. Moreover, according to the Bragg's law, wurtzite peaks in bare ZnO NPs lie at higher diffraction angles than ZnO/SiO_2_H_2O NPs, indicating a smaller lattice spacing within the nanostructure, probably connected to the occurrence of oxygen vacant regions. Along the same line, the shift of the reflections of ZnO/SiO_2_H_2O towards lower 2θ values envisages the presence of zinc interstitial species in the oxide lattice, leading to larger interplanar distances.

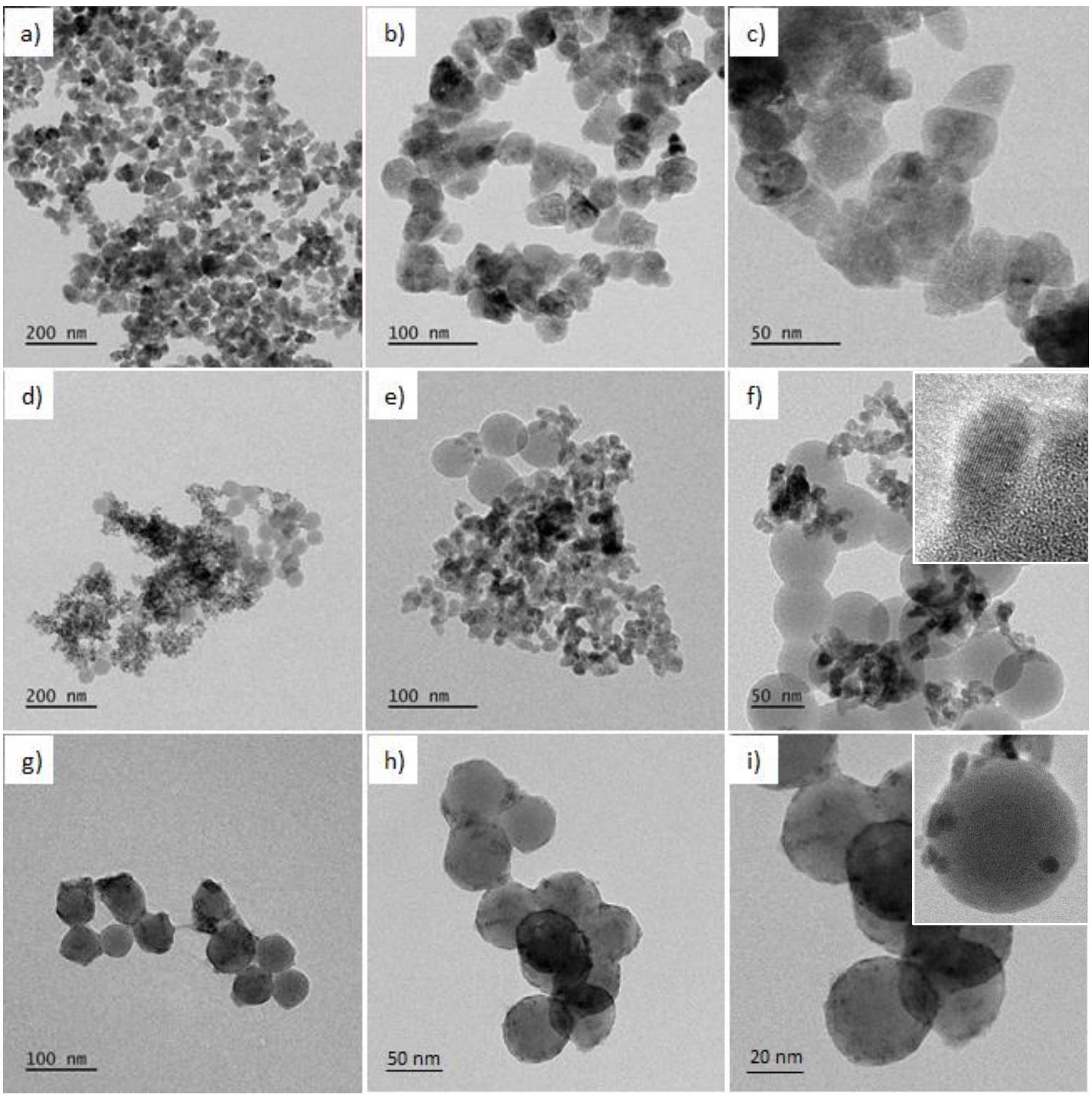

Figure 2. TEM images of: a)-c) bare ZnO NPs; d)-f) ZnO/SiO_2_H_2O and g)-i) ZnO/SiO_2_EtOH. Inset in f) and i) highlights the ZnO NPs anchored on the surface of amorphous silica.

The morphological features of ZnO and ZnO/SiO_2 samples were investigated by TEM (Figure 2). In detail, the images reveal that bare ZnO is constituted by micrometric or submicrometric agglomerates of irregularly shaped NPs (Figure 2a) with average length of ~ 30-40 nm (Figure 2b, c). In the case of ZnO/SiO_2_H_2O, separate aggregates can be observed (Figure 2d), where small ZnO NPs (average diameter of ~ 10-15 nm) cover or bridges the larger silica nanospheres (Figure 2e,f). High resolution images (HRTEM, inset in Figure 2f) allow to identify the presence in ZnO NPs of lattice fringes with interplanar distance of ~ 0.28 nm, corresponding to (100) atomic planes, thus corroborating the crystallinity assessed by PXRD.

For ZnO/SiO_2_EtOH TEM images show silica nanospheres uniformly decorated by very tiny and amorphous ZnO NPs (Figure 2g,h), whose occurrence can be revealed only at very large magnifications (Figure 2i and inset). Also in this case, the results of TEM images are in agreement with those retrieved by PXRD pattern.

UV-Vis spectroscopy was performed to further confirm the generation of ZnO NPs in ZnO/SiO_2 systems (Figure 3).

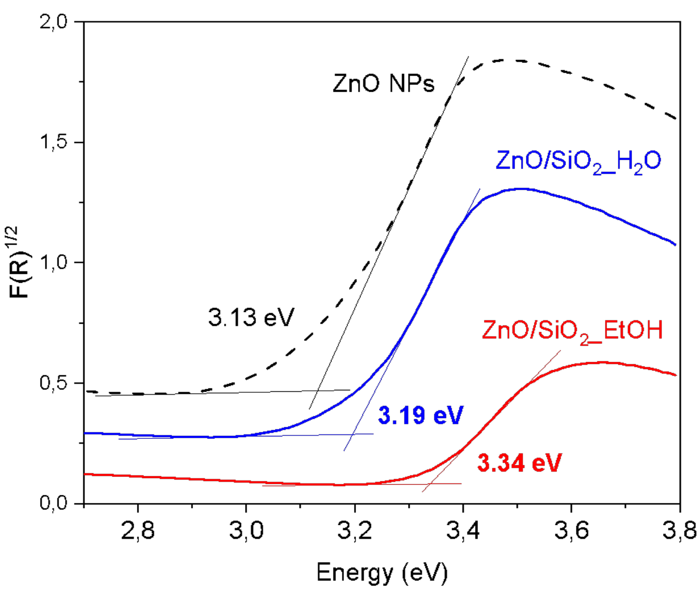

Figure 3. UV-Vis spectra of bare ZnO NPs (black-line), ZnO/SiO_2_EtOH (red-line) and ZnO/SiO_2_H_2O (blue-line) systems elaborated according to the Kubelka Munk equation [25]. The intercept between the tangents to the curve slope and the minimum value corresponds to the E_g value.

For ZnO/SiO_2_H_2O sample, where the largest ZnO NPs are present, a band gap energy (Eg = 3.19 eV) very similar to that of bulk ZnO is observed. Conversely, a progressive energy blue-shift is detectable for ZnO/SiO_2_EtOH (Eg = 3.34 eV), corroborating the smaller ZnO NPs dimensions revealed by TEM for this activator. These results are in agreement with our previous investigation on mesoporous silica NPs decorated by ZnO [20, 21] and support the presence of the oxide NPs in ZnO/SiO_2_EtOH.

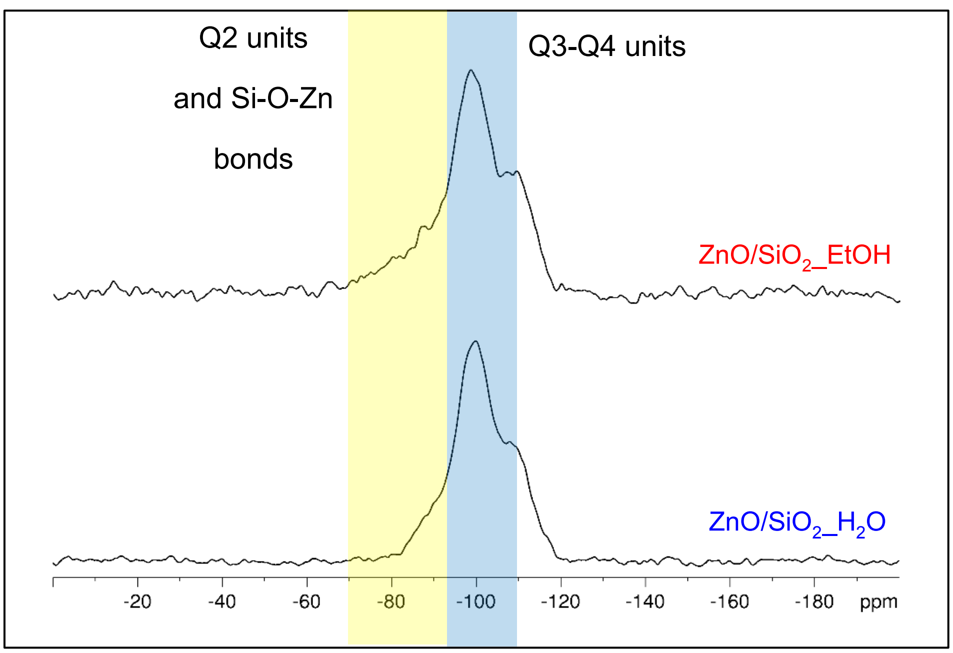

Figure 4. ^{29}Si CPMAS NMR spectra of ZnO/SiO_2_EtOH (above) and ZnO/SiO_2_H_2O (below).

In order to study the interaction between ZnO NPs and SiO_2 with a particular focus on the Si-O-Zn bond formation, the ^{29}Si CPMAS spectra of the ZnO/SiO_2 systems are reported (Figure 4). Both spectra are characterized by the Q signal that can be fitted with the silica Q^4 and Q^3 resonances between -90 and -110 ppm, together with a superimposition of a broad shoulder in the range from -70 to -90 ppm, which could account for both silica Q^2 resonance and signals due to Si units substituted with a variable number of Si-O-Zn bonds [20].

An in depth semi-quantitative analysis of the CPMAS spectra has been performed in order to inspect potential differences in the anchoring of ZnO at the silica surface. The results are summarized in Table 1. As stated above, the Q resonance can be adequately fitted with 5 components centred at about -109, -100, -94, -88, -81 and -74 ppm. By comparison with the ^{29}Si spectrum of the bare SiO_2 NP (not shown), the components at -109, -100 and -88 ppm are assigned to Q^4, Q^3 and Q^2 silica units. Consequently, the other components represent the partial substitution of Si-O-Si and Si-OH bonds with Si-O-Zn bonds on the particle surface (Q^nZn_m units, with m number of Zn bonded to a SiO_4 unit), proving the effective anchoring of the ZnO NPs [21]. This is indirectly confirmed by the reduction of surface Q^3 units compared to bare SiO_2 (see Table 1). Moreover, the presence of additional Q_nZn_m components (at -74 and -81 ppm) in the ZnO/SiO_2_EtOH spectrum indicates a more efficient anchoring compared to ZnO/SiO_2_H_2O.

Table 1. ^{29}Si CP-MAS NMR semi-quantitative results: relative amount and assignment of the main identified units.

Assign.		**Q^nZn_m**	**Q^nZn_m**	**Q2/ Q^nZnm**	**Q^nZn_m**	**Q3**	**Q4**
δ(iso)		*-74,3*	*-80,9*	*-87,9*	*-93,7*	*-99,7*	*-109,5*
SiO_2	%	--	--	12,7	--	67,6	19,7
ZnO/SiO_2_H_2O	%	--	--	7,8	11,9	50,4	29.9
ZnO/SiO_2_EtOH	%	3,6	3,7	10,9	9,4	45,7	26,8

It is worth to mention that Table 1 reports only an attempt of attribution. As a matter of facts, the substitution, with consequent changes in the torsion angles T-Ô-T (T stands for a generic cation), pushes downfield the related resonances with respect to the pure components [26], but both the small shift and the intrinsic broadness of the components prevent the possibility of a definite assignment of substituted Q^n unit.

These data drove to the conclusion that a different anchoring of the ZnO NPs on the silica surface was obtained according to the synthetic conditions. The spectrum of ZnO/SiO_2_EtOH sample, characterized by mainly small amorphous ZnO NPs, shows a wider left shoulder in the range -70 to -100 ppm, due to the higher presence of Si-O-Zn components, with respect to ZnO/SiO_2_H_2O sample (decorated with both amorphous and crystalline ZnO NPs, that tend to aggregate). This result suggests that both the NPs size and aggregation remarkably influence the growth and distribution of ZnO on SiO_2 surface.

XPS analysis was carried out to further study the surface composition of the prepared ZnO/SiO_2 systems. The typical XPS wide survey spectra of ZnO/SiO_2 samples and of the reference pure ZnO sample are showed in Figure S1 of the Supporting Information (SI), which reports the Zn, O and C detected peaks. The presence of C in the samples may be ascribed both to residual acetate species derived from the Zn precursor utilized for the materials synthesis and to the adventitious carbon adsorbed on the surface during the exposure of the samples to the ambient atmosphere. The BE values were corrected for the charge shift using as a reference the C 1s peak of graphitic carbon (BE = 284.8 eV). Figure 5a displays the Zn $2p_{3/2}$ XPS spectra of ZnO, ZnO/SiO_2_EtOH and ZnO/SiO_2_H_2O. While in pure ZnO, the Zn $2p_{3/2}$ level is detected at BE ~ 1021.7 ± 0.2 eV typical of Zn−O ionic binding in agreement with the literature [27], for ZnO/SiO_2 activators is found at slightly higher BE ~1022.1 ± 0.2 eV. This shift to higher BE suggests a change in the binding state of Zn ions, which can be induced by the formation of Zn–O–Si bonds at the interface between the ZnO and SiO_2 NPs in ZnO/SiO_2 samples and/or to non-linear charging effects often observed in insulating samples [28] (not accounted by the alignment of the spectra at C 1s peak mentioned above). Moreover, a contribution deriving from Zn species in ZnO(OH) or Zn(OH) environment cannot be excluded, particularly for ZnO/SiO_2_EtOH system [21].

Spectra deconvolution (Figure 5a) enables to notice the presence of another component, located at lower BE (~ 1020.0 ± 0.2 eV), which appears much more relevant in ZnO/SiO_2_H_2O. The overall shift of Zn $2p_{3/2}$ core level to lower BE in ZnO-based materials usually reflects a change in the binding state of Zn ions, which can be ascribed to a different coordination in the oxide lattice or to a loss in the number of oxygen ions in nanocrystalline ZnO (i.e. oxygen defects) [29, 30]. However, it has to be mentioned also that the presence of zinc interstitials species near the surface of ZnO may contribute to the depletion of BE value [29].

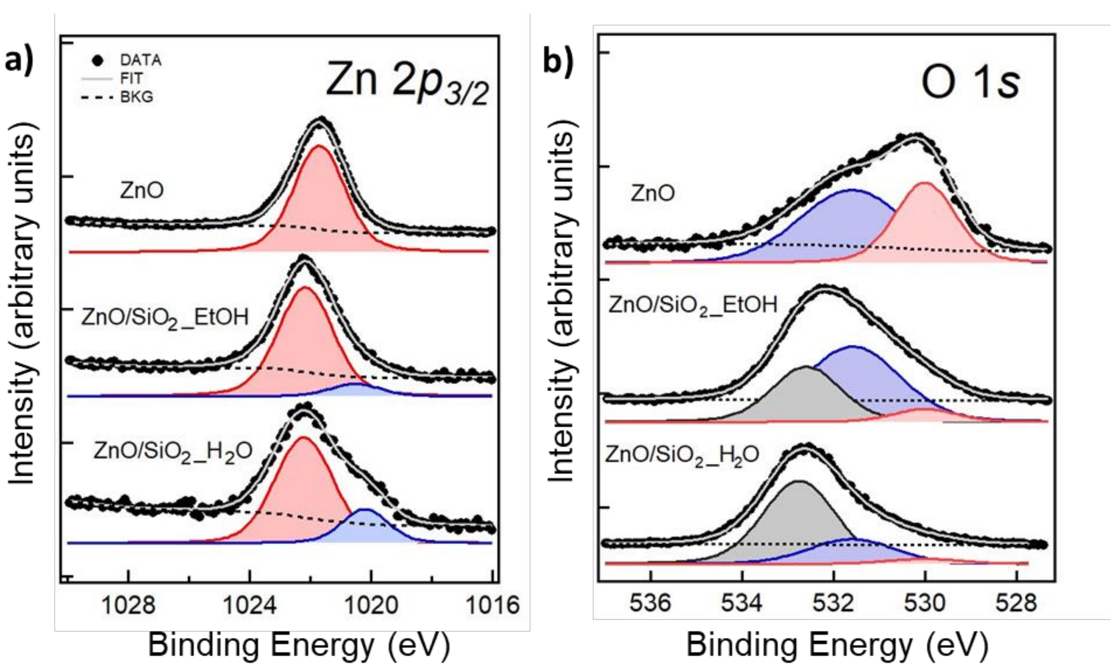

Figure 5. a) Zn 2*p3/2* and b) O 1*s* XPS spectra of ZnO, ZnO/SiO_2_EtOH and ZnO/SiO_2_H_2O samples.

O 1*s* XPS spectra of ZnO, ZnO/SiO_2_EtOH and ZnO/SiO_2_H_2O samples (Figure 5b) display remarkable differences. The O 1*s* level in ZnO is significantly broad, suggesting the occurrence of oxygen species in a different chemical environment. Indeed, spectral deconvolution results in different bands centered at 530.0 ± 0.2 eV and 531.6 ± 0.2 eV (Figure 5b), which are assigned to lattice oxygen ($O_{lattice}$) in the wurtzite structure and to ZnO(OH)/Zn(OH) species, respectively [31]. Besides the occurrence of $O_{lattice}$ and ZnO(OH)/Zn(OH), an additional peak at 533.0 ± 0.2 eV can be revealed by fitting ZnO/SiO_2 spectra (Figure 5b), which is attributable to loosely bound oxygen in the amorphous SiO_2 NPs or partially weakly adsorbed oxygen species such as water [32]. Accordingly, this latter contribution appears more evident in ZnO/SiO_2_H_2O than in ZnO/SiO_2_EtOH NPs where, instead, the band related to ZnO(OH)/Zn(OH) species dominates the spectrum (Figure 5b). In summary, the XPS survey thus unveils significant differences between the surfaces properties of ZnO/SiO_2 systems, which may envisage a specific reactivity.

Study of the SA interaction with ZnO/SiO_2 samples

In the first step of the vulcanization mechanism ZnO interacts with SA leading to reactive Zn(II)-SA adducts which, upon reaction with the accelerator and sulfur, provide Zn complexes bearing polysulfidic ligands, behaving as the active sulfurating agents [1-11].

In an attempt to mimic this initial passage, the interaction between SA and ZnO/SiO_2 systems was explored through DSC. In detail, following the seminal works on the argument carried out by Kruger and McGill [33-34], the measurements were performed in the solid-state by mixing the samples with SA and then heating to the conventional temperature conditions experienced during the vulcanization process. Results are summarized in Figure 6.

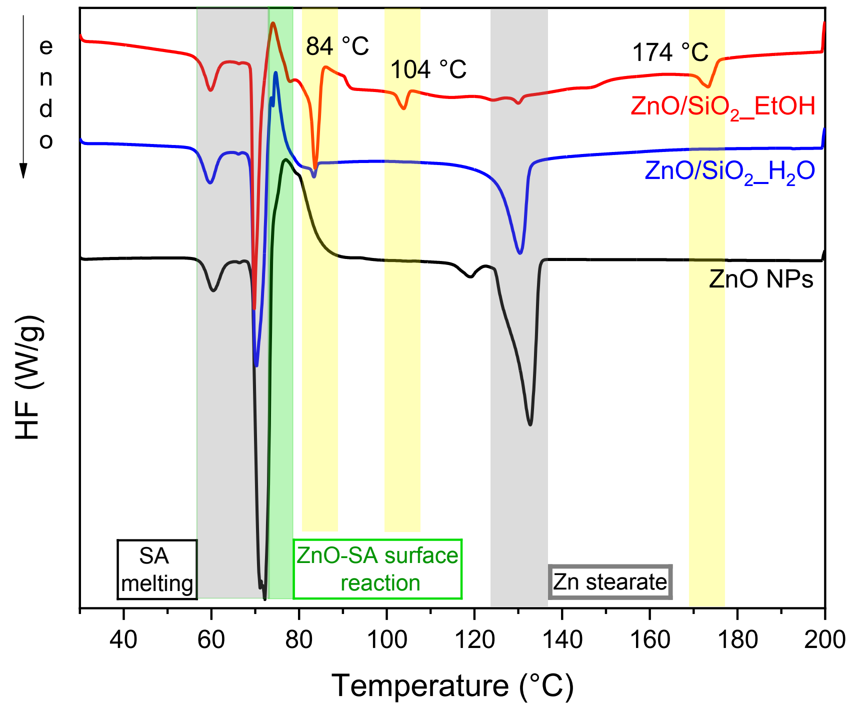

Figure 6. DSC curves of ZnO and ZnO/SiO_2 samples mixed with SA in the temperature range of 30-200°C.

During the first heating ramp, for both bare ZnO and ZnO/SiO_2 samples (Figure 6), an endothermic phenomenon in the temperature range 60-72 °C connected to the melting of free SA was observed [33], followed by an exothermic peak at ~ 80 °C. This was associated to the possible surface interaction between ZnO and SA, that occurs when the liquid SA gets closer to the surface of ZnO NPs. Besides, an additional endothermic peak at ~ 130 °C appears in all samples, probably associated to the melting of one of the reaction products, followed by its crystallization at ~ 115 °C during the cooling ramp (Figure S2a) and its further melting in the last heating ramp (Figure S2b). Interestingly, after the first heating ramp, ZnO/SiO_2 samples show the peak corresponding to that of the melting temperature typical of zinc stearate and no peaks due to SA, suggesting its total consumption. However, in the case of ZnO/SiO_2_EtOH, three new endothermic peaks are observed at 84, 104 and 174 °C, still present in the second heating ramp along with a small peak due to zinc stearate. This suggests a peculiar reactivity of ZnO/SiO_2_EtOH with SA, which opens the pathway to the formation of reaction products with distinctive structural properties, most likely promoted by the diverse structural and surface properties of ZnO NPs.

Further insights on the products originated by ZnO-SA interaction were collected through TGA analysis, which was performed after DSC treatment. In detail, TGA curve of ZnO NPs interacted with SA reveals two main contributions to the weight loss (Figure 7, grey bands), ascribable to residual SA (T_{onset} = 150 °C) and zinc stearate (T_{onset} = 260 °C), respectively.

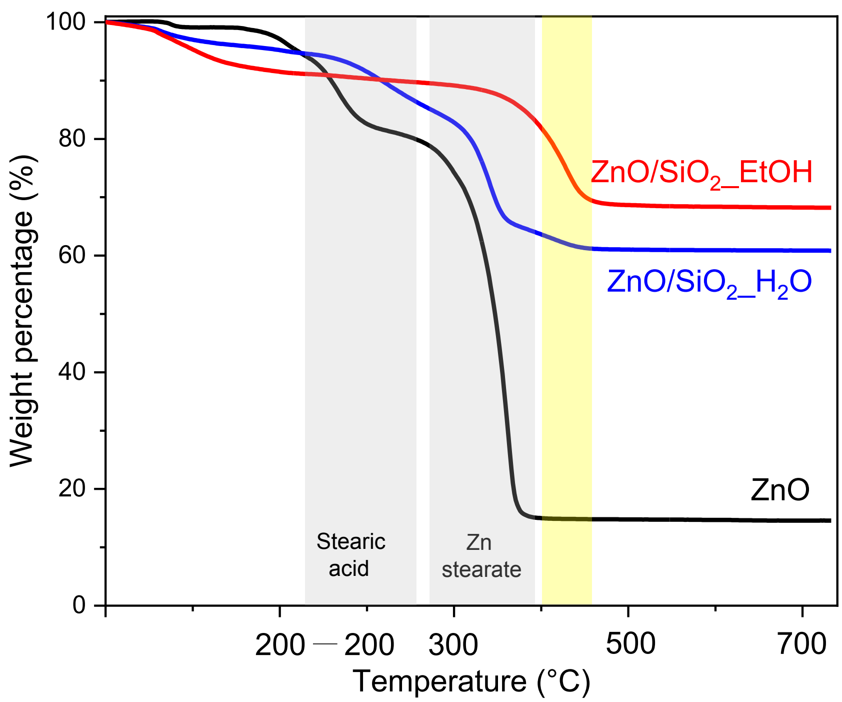

Figure 7. Thermal degradation profiles of the reaction products formed after the interaction of ZnO/SiO_2 samples with SA, compared to ZnO NPs interacted with SA. Grey bands evidence the typical weight loss due to SA and Zn stearate. In yellow the presence of an additional component with higher thermal stability is evidenced.

Reference thermal profiles of both SA and zinc stearate are reported in Figure S3. Similar indications were obtained for ZnO/SiO_2_H_2O sample, where a small additional weight loss at T_{onset} = 390 °C is detected too (Figure 7, yellow band). However, this latter contribution becomes predominant in the case of ZnO/SiO_2_EtOH, where no weight losses due to SA and zinc stearate were observed, thus confirming that the interaction of SA with ZnO/SiO_2_EtOH promotes the generation of different reaction products characterized by a higher thermal stability than that of zinc stearate.

The structural properties of the reaction products were preliminarily investigated by FTIR spectroscopy (Figure 8). Spectrum of ZnO NPs interacted with SA (Figure 8, black line) exhibits the main features of both SA and zinc stearate. In fact, the intense peak at 1750 cm^{-1} and the two bands at 1538 cm^{-1} and 1398 cm^{-1} are assigned to the C=O stretching of COOH groups due to free SA and to the asymmetric and symmetric stretching of COOH coordinated to zinc centers in the structure of zinc stearate, respectively. This supports the formation of zinc stearate as the main intermediate species generated in the first vulcanization steps, through the solubilization of Zn centers of ZnO with SA. When ZnO/SiO_2 samples were reacted with SA, no residual SA was detected at the end of the reaction, suggesting a possible higher reactivity of these systems compared to bare ZnO. Indeed, signals ascribable to different reaction products appeared in the spectra of both ZnO/SiO_2_H_2O and ZnO/SiO_2_EtOH (blue and red lines in Figure 8, respectively). In particular, ZnO/SiO_2_H_2O reacted with SA shows: i) the typical signals at 1538 and 1398 cm^{-1} assigned to the zinc stearate structure; ii) additional peaks at 1622, 1609 and 1595 cm^{-1}, along with vibrations at 1420 and 1411 cm^{-1} possibly connected to surface zinc complexes with different structure. In the case of ZnO/SiO_2_EtOH, the peaks of zinc stearate were completely absent and replaced by an intense band at 1560 cm^{-1}, adjacent to the very weak vibrations at 1622 and 1609 cm^{-1}, already observed in ZnO/SiO_2_H_2O.

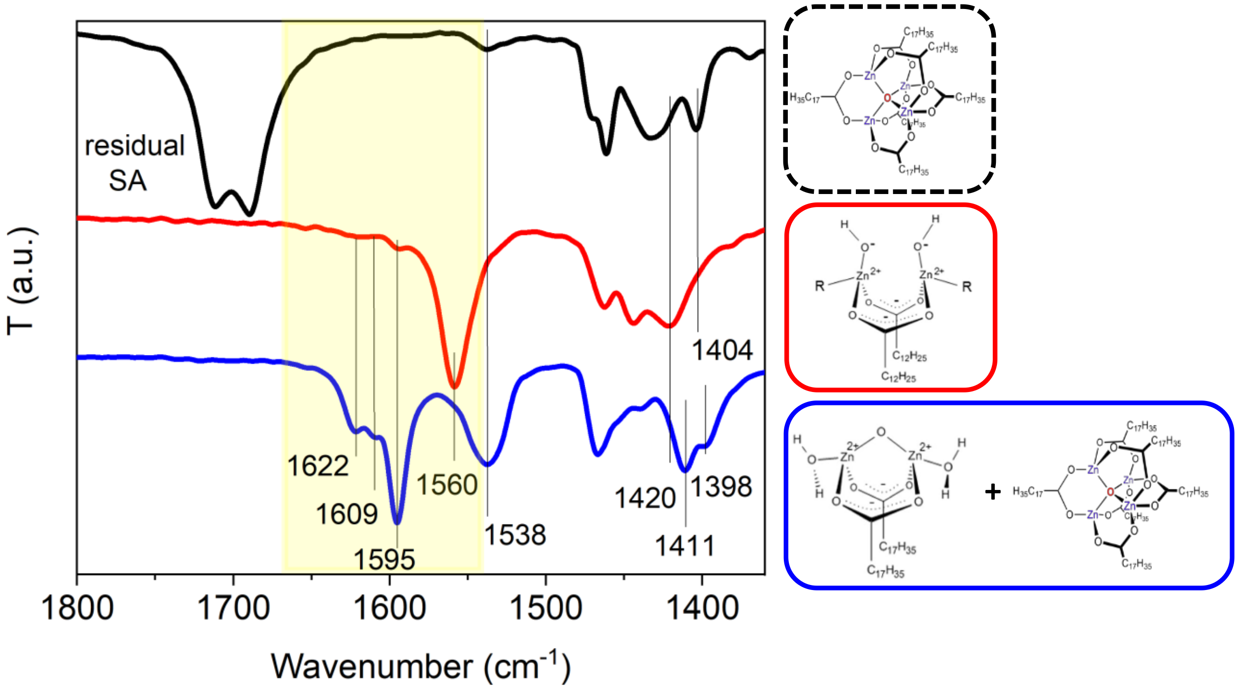

Figure 8. FTIR spectra of ZnO NPs (black line), ZnO/SiO_2_H_2O (blue line) and ZnO/SiO_2_EtOH (red line) samples after the interaction with SA. The possible SA-ZnO structure are illustrated for each sample on the side of the spectrum.

According to Ikeda et al. [14], the spectral features of ZnO/SiO_2 NPs indicate the presence of dinuclear bridging bidentate coordinated zinc/stearate complexes, where each SA molecule connects two zinc centers with a Zn:SA molar ratio equal to 1:1, leaving two free positions on each Zn(II) sites for further ligands. In detail, for ZnO/SiO_2_H_2O, the vibrations resemble those attributed to a skeleton composed of $[Zn_2(\mu\text{-}O_2CC_{17}H_{35})_2]^{2+}$•4X, where X is hydroxyl group, water and/or acetate ligands (see Inset in Figure 8, red square). Instead, the further shift of the COO^- stretching towards lower wavenumber observed for ZnO/SiO_2_EtOH, may be justified considering the formation of a bridged oxo group between two zinc atoms instead of two hydroxyl groups and/or acetate ligands (Inset in Figure 8, blue square). In addition, the peak at 1622 cm^{-1} detected in both SiO_2/ZnO samples can be identified with non-bridged monodentate structures [35].

These results, besides matching with several previous studies [14-15, 20-21], endorse the generation of different reaction products due to the SA interaction with ZnO/SiO_2 activators, in line with DSC and TGA data.

The SA reactivity with ZnO/SiO_2 systems was further deepen by investigating the local binding modes of the carboxylic acid at the oxide interface through ^{13}C solid state NMR. The spectra of both ZnO/SiO_2 samples treated with SA and the pure SA are reported in Figure 9.

All the resonances belonging to SA are clearly detectable in the samples, with a slightly broader shape than for the pure acid, due to a reduced mobility typical of the grafting process [36]. Most interestingly, the carbonyl resonance (**1**) of SA at 180 ppm is both downfield shifted and split to 185 and 183 ppm in ZnO/SiO_2 systems. As this resonance represents a spectroscopic signature of the binding mode of the carboxylic group to the metal oxide surface [36], the formation of the zinc stearate complexes after ZnO-SA interaction was further confirmed. Moreover, the presence of two signals indicates two possible geometries for the coordination of the fatty acid to the metal centre [36-40] but the assignment to specific binding modes is not trivial.

As a matter of fact, according to the literature, the peak at 185 ppm could correspond to chelating carboxylate carbons, whereas the 183 ppm signal could be assigned to dinuclear bidentate bridging carboxylate carbons [36-40] or, in better agreement with IR results, they both could refer to bidentate bridging $[Zn_2(\mu\text{-}O_2CC_{17}H_{35})_2]^{2+}$•4X with different X ligands. From a closer inspection, these two resonances are present in the two samples with different ratios, equal to 51:40 and 96:4, for ZnO/SiO_2_EtOH and ZnO/SiO_2_H_2O respectively. The different coordination mode is reflected by the downfield shifted and doubled resonance of the α-CH_2 groups (**2**), which moves from 34.3 ppm in SA to 39.7 and 42.1 ppm in both ZnO/SiO_2 samples [36]. The similarity of all the other resonance indicates that the chain packing does not change among the samples.

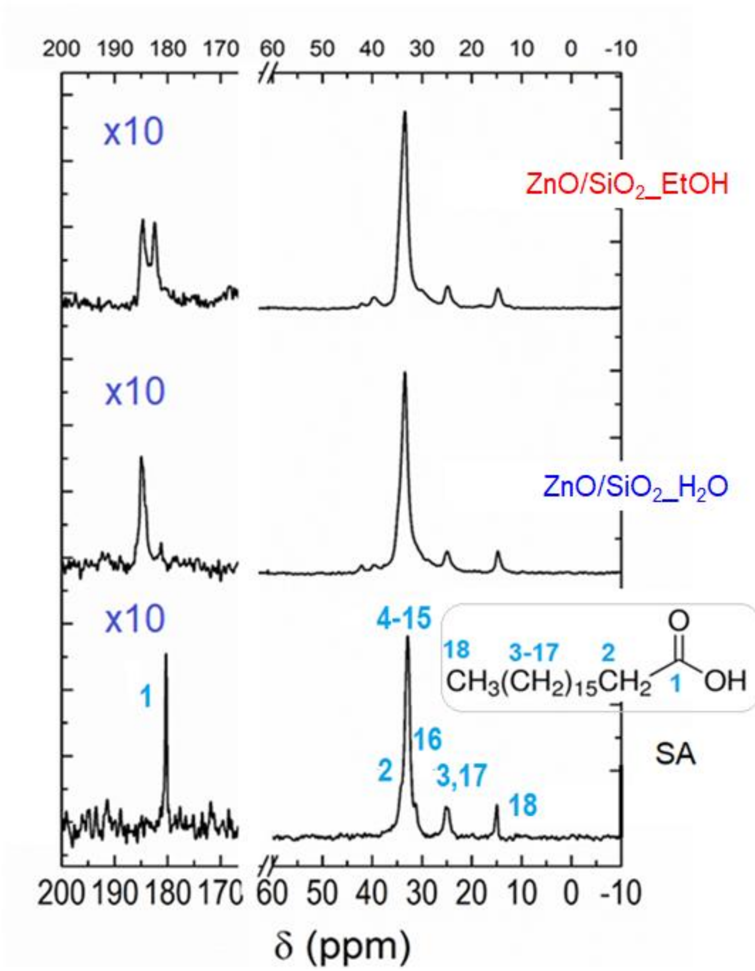

Figure 9. ^{13}C CPMAS NMR spectra of the ZnO/SiO_2 samples after SA interaction, compared with pure SA.

The above outcomes enable us to complete the picture drawn by DSC, TGA and FTIR analyses, highlighting the occurrence of a peculiar reactivity for ZnO/SiO_2 systems with SA, evidently connected to their structural, morphological and surface characteristics.

In particular, ZnO/SiO_2_EtOH NPs with poor crystallinity, tiny particle size and remarkable presence of ZnO(OH)/Zn(OH) at the surface seems to promote the generation of ZnO-SA bridging bidentate structures with high thermal stability. Conversely, the higher crystallinity, larger particle size and lattice defectivity of ZnO/SiO_2_H_2O NPs drive the reaction with SA towards the formation of a mixture of Ikeda-like complexes [14, 15] and other Zn stearate structures, with a generally lower thermal stability.

These considerations are in agreement with both theoretical and experimental studies reported in the literature, where carboxylate species on ZnO surfaces are found mostly adopting the most thermodynamically favored bidentate configuration, whereas other adsorption configurations are recognized only in the presence of defective sites (e.g. oxygen vacancies), like those detected by XPS in ZnO/SiO_2_H_2O NPs. Moreover, previous reports on similar oxide systems describe a correlation between the occurrence of OH groups at the ZnO surface and the bridging bidentate configuration obtained upon interaction of SA with ZnO/SiO_2_EtOH.

The generation and the chemical structure of these specific Zn(II)-SA vulcanization intermediates was finally related to the peculiar behavior imparted by ZnO/SiO_2_EtOH and ZnO/SiO_2_H_2O activators to the curing of silica/isoprene NCs, as reported in Figure 10. In detail, the vulcanization curves were registered by measuring the torque (S’) values over the curing time and the performance were compared to that of conventionally IR NCs prepared using microcrystalline ZnO. The sulfur cross-link formation between polymer chains is responsible for the higher viscosity of the vulcanized materials and is connected to the measured S’ increase.

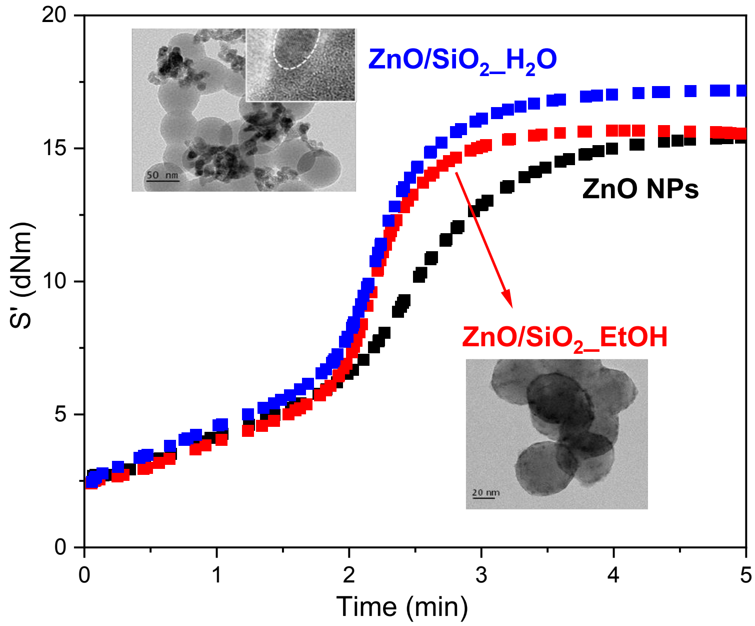

Figure 10. Vulcanization curves measured for silica/IR NCs vulcanized with ZnO/SiO_2_EtOH and ZnO/SiO_2_H_2O activators, compared to bare ZnO.

Comparing the curves, both ZnO/SiO_2 materials show higher maximum torque (M_{max}) and are characterized by a lower curing time (t_{90}, the time required for reaching 90% of M_{max} at the curing temperature) compared to pure ZnO. Moreover, an appreciable difference between the M_{max} values of ZnO/SiO_2_EtOH and ZnO/SiO_2_H_2O can be observed (Fig. 10), suggesting a distinct ability of the Zn(II)-SA complexes in supplying Zn(II) centers readily interacting with the other curing agents. However, clarifying the reason behind this difference is notoriously difficult, since it entails several other parameters influencing the vulcanization process, and it is currently part of an ongoing investigation.

Nevertheless, the overall results point out that morphology and surface control of the ZnO activators enable not only a peculiar reactivity with stearic acid, but remarkably impact also on the vulcanization performance delivered to the resulting rubber nanocomposites.

CONCLUSION

In this manuscript, we have studied the influence of the structural, morphological and surface features of different ZnO/SiO_2 activators on their reactivity with SA, trying to gain valuable information connected to the first step of the vulcanization mechanism.

Pursuing this target, a comprehensive characterization was initially performed through XRD and TEM, which evidenced an effect of reaction solvent, EtOH or water, in providing amorphous and tiny particles decorating SiO_2 nanospheres or crystalline and large ZnO nanocrystals bridging the silica aggregates, respectively.

^{29}Si solid state NMR and, more in depth, XPS investigation corroborated a distinct anchoring of ZnO on the silica surface of ZnO/SiO_2 systems, unveiling the occurrence of inequivalent surface properties: ZnO(OH)/Zn(OH) species dominating in ZnO/SiO_2_EtOH NPs while oxygen defects in ZnO/SiO_2_H_2O NPs. These characteristics lead to significant fallouts in the reactivity with SA, which was performed and monitored by DSC. Different thermal events have been retrieved, which, according to FTIR, TGA and ^{13}C NMR correspond to unique reaction products both in terms of chemical architecture and of thermal stability. In detail, while for pure ZnO only zinc stearate represents the exclusive detected species, unequal ZnO-SA bridging bidentate complexes, very similar to those proposed by Ikeda and co-workers and described as determinant for the vulcanization process, have been observed for SiO_2/ZnO NPs.

The chemical structure of these specific Zn(II)-SA vulcanization intermediates was finally proved to be involved in the peculiar curing behavior imparted by ZnO/SiO_2_EtOH and ZnO/SiO_2_H_2O activators to silica/isoprene NCs.

The overall results suggest that careful tailoring of the features of ZnO activators offers the chance to orient the initial step of the vulcanization mechanism toward the generation of specific

Zn(II)-SA intermediates, which significantly boost the yield of the curing process, with potential economic and environmental benefits.

Finally, the methodological protocol adopted in this study may help to critically complement the outstanding results already reported in the literature, by proposing a valid benchmark for achieving further insights on the interaction of SA with activators, and in turn, with the other species involved in the vulcanization mechanism.

ASSOCIATED CONTENT

Supporting Information. XPS wide survey spectra of ZnO and ZnO/SiO_2 samples; DSC curves registered during the cooling ramp (200-30 °C) and the second heating ramp (30-200 °C); Thermal profiles of zinc stearate and SA.

AUTHOR INFORMATION

Corresponding Author

* Prof. Massimiliano D’Arienzo, email: massimiliano.darienzo@unimib.it, phone number: 0039-026448-5023

Author Contributions

The manuscript was written through contributions of all authors. All authors have given approval to the final version of the manuscript.

ACKNOWLEDGMENTS

This work was in the frame of the EU upscaling project SAFE-VULCA (reference number 18145, 2019-2021) funded by the European Institute of Innovation and Technology (EIT) Raw Materials, a body of the European Commission, under the Horizon 2020, the EU Framework Program for Research and Innovation. We thank Dr. Antonio Luca Berardino for its contribution to this work during the internship for his master's degree.

ABBREVIATIONS

SA stearic acid; NPs nanoparticles; TEM Transmission Electron Microscopy; DSC Differential Scanning Calorimetry; FTIR Fourier Transform Infrared Spectroscopy; NMR Nuclear Magnetic Resonance; XPS X-ray Photoelectron Spectroscopy.

REFERENCES

[1] C.M. Blow, C. Hepburn, *Rubber Technology and Manufacture*, Butterworth Scientific, London (1981), 2nd Ed.

[2] W. Hofmann, *Rubber Technology Handbook*, Hanser Publishers, New York (1994).

[3] M. Coleman, J. R. Shelton, J. L. Koenig. Sulfur Vulcanization of Hydrocarbon Diene Elastomers. *Ind. Eng. Chem. Prod. Res. Dev.* 13 (1974) pp 154 –166

[4] M. R. Krejsa, J. L. Koenig. A Review of Sulfur Crosslinking Fundamentals for Accelerated and Unaccelerated Vulcanization. *Rubber Chem. Technol.* 66 (1993) pp 376 – 410

[5] F. Ignatz-Hoover. Review of Vulcanization Chemistry. *Rubber World* 220 (1999) pp 24

[6] P. J. Nieuwenhuizen. Zinc Accelerator Complexes. Versatile Homogeneous Catalysts in Sulphur Vulcanization. *Appl. Catal. A Gen.* 207 (2001) pp 55 – 68

[7] G. Heideman, R. N. Datta, J. W. M. Noordermeer, B. Van Baarle. Activators in Accelerated Sulphur Vulcanization. *Rubber Chem. Technol.* 77 (2004) pp 512 – 541

[8] G. Heideman, R. N. Datta, J. W. M. Noordermeer, B. Van Baarle. Influence of Zinc Oxide during Different Stages of Sulphur Vulcanization Elucidated by Model Compound Studies. *J. Appl. Polym. Sci.* 95 (2005) pp 1388 – 1404

[9] Y. Ikeda, A. Kato, S. Kohjiya, Y. Nakajima. *Rubber Science: A Modern Approach*, Springer, Singapore (2017)

[10] S. Mostoni, P. Milana, B. Di Credico, M. D'Arienzo, R. Scotti. Zinc-Based Curing Activators: New Trends for Reducing Zinc Content in Rubber Vulcanization Process. *Catalysts* 9 (2019) pp 664

[11] G. Heideman. Reduced Zinc Oxide Levels in Sulphur Vulcanisation of Rubber Compounds. *Ph.D. Thesis*, University of Twente, Enschede, The Netherlands (2004)

[12] Coran, A. Y. 7 - Vulcanization. In *Science and Technology of Rubber* (Second ed.); Mark, J. E.; Erman, B.; Eirich, F. R., Eds.; Academic Press: San Diego, 1994; pp 339 – 385.

[13] P. Ghosh, S. R. Katare, P. R. Patkar, J. M. Caruthers, V. Venkatasubramanian, K. A. Walker. Sulfur Vulcanization of Natural Rubber for Benzothiazole Accelerated Formulations: From reaction mechanisms to a rational kinetic model. *Rubber Chem. Technol.* 76 (2003) pp 592 – 693

[14] Y. Ikeda, Y. Yasuda, T. Ohashi, H. Yokohama, S. Minoda, H. Kobayashi, T. Honma. Dinuclear Bridging Bidentate Zinc/Stearate Complex in Sulfur Cross-Linking of Rubber. *Macromolecules* 48 (2015) pp 462 – 475

[15] Y. Ikeda, Y. Sakaki, Y. Yasuda, P. Junkong, T. Ohashi, K. Miyaji, H. Kobayashi. Roles of Dinuclear Bridging Bidentate Zinc/Stearate Complexes in Sulfur Cross-Linking of Isoprene Rubber. *Organometallics* 38 (2019) pp 2363 – 2380

[16] Y. Ikeda, N. Higashitani, K. Hijikata, Y. Kokubo, Y. Morita, M. Shibayama, N. Osaka, T. Suzuki, H. Endo, S. Kohjiya. Vulcanization: New Focus on a Traditional Technology by Small-Angle Neutron Scattering. *Macromolecules* 42 (2009) pp 2741 – 2748

[17] Y. Yasuda, S. Minoda, T. Ohashi, H. Yokohama, Y. Ikeda. Two-Phase Network Formation in Sulfur Crosslinking Reaction of Isoprene Rubber. *Macromol. Chem. Phys.* 215 (2014) pp 971 – 977

[18] P. Junkong, R. Morimoto, K. Miyaji, A. Tohsan, Y. Sakaki, Y. Ikeda. Effect of fatty acids on the accelerated sulfur vulcanization of rubber by active zinc/carboxylate complexes. *RSC Adv.* 10 (2020) pp 4772 – 4785

[19] M. Hernández, T. A. Ezquerra, R. Verdejo, M. A. López-Manchado. Role of Vulcanizing Additives on the Segmental Dynamics of Natural Rubber. *Macromolecules* 45 (2012) pp 1070–1075

[20] A. Susanna, L. Armelao, E. Callone, S. Dirè, M. D'Arienzo, B. Di Credico, L. Giannini, T. Hanel, F. Morazzoni, R. Scotti. ZnO Nanoparticles Anchored to Silica Filler. A Curing Accelerator for Isoprene Rubber Composites. *Chem. Eng. J.* 275 (2015) pp 245 – 252

[21] A. Susanna, M. D'Arienzo, B. Di Credico, L. Giannini, T. Hanel, R. Grandori, F. Morazzoni, S. Mostoni, C. Santambrogio, R. Scotti. Catalytic Effect of ZnO Anchored Silica Nanoparticles on Rubber Vulcanization and Cross-Link Formation. *Eur. Polym. J.* 93 (2017) pp 63 – 74

[22] S. Mostoni, M. D'Arienzo, B. Di Credico, L. Armelao, M. Rancan, S. Dirè, E. Callone, R. Donetti, A. Susanna, R. Scotti. Design of a Zn Single-Site Curing Activator for a More Sustainable Sulfur Cross-Link Formation in Rubber. *Industrial & Engineering Chemistry Research* 60 (2021) pp 10180 – 1019

[23] T. Wu, Y. Zhang, X. Wang, S. Liu. Fabrication of Hybrid Silica Nanoparticles Densely Grafted with Thermoresponsive Poly(N-isopropylacrylamide) Brushes of Controlled Thickness via Surface-Initiated Atom Transfer Radical Polymerization. *Chem. Mater.* 20 (2008) pp 101 – 109

[24] W. Stöber, A. Fink, E. Bohn. Controlled growth of monodisperse silica spheres in the micron size range. *J. Colloid Interface Sci.* 26 (1068) pp 62 – 69

[25] S. Monticone, R. Tufeu, A. V. Kanaev. Complex nature of the UV and visible fluorescence of colloidal ZnO nanoparticles. *J. Phys. Chem. B* 102 (1998) pp 2854 – 2862

[26] C. Bertail, S. Maron, V. Buissette, T. Le Mercier, T. Gacoin, J. P. Boilot. Structural and Photoluminescent Properties of Zn2SiO4:Mn2+ Nanoparticles Prepared by a Protected Annealing Process *Chem. Mater.* 23 (2011) pp 2961 – 2967

[27] M. A. Mahjoub, G. Monier, C. Robert-Goumet, F. Réveret, M. Echabaane, D. Chaudanson, M. Petit, L. Bideux, B. Gruzza. Synthesis and study of stable and size-controlled ZnO–SiO_2 quantum dots: application as a humidity sensor. *J. Phys. Chem. C* 120 (2016) pp 11652– 11662

[28] J. F. Moulder, W. F. Stickle, P. E. Sobol, K. D. Bomben. In *Handbook of X-ray Photoelectron Spectroscopy*; Chastain, G., Ed.; Perkin Elmer Corporation: Eden Prairie (Minnesota), 1992.

[29] Y. Y. Tay, S. Li. Size dependence of Zn 2*p* 3/2 binding energy in nanocrystalline ZnO. *Appl. Phys. Lett.* 88 (2006) pp 173118

[30] F. M. Chang, S. Brahma, J. H. Huang, Z. Z. Wu, K. Y. Lo. Strong correlation between optical properties and mechanism in deficiency of normalized self-assembly ZnO nanorods. *Sci Rep* 9 (2019) pp 905

[31] L. L. Yang, Q. X. Zhao, M. Willander, X. J. Liu, M. Fahlman, J. H. Yang. Origin of the surface recombination centers in ZnO nanorods arrays by X-ray photoelectron spectroscopy. *Applied Surface Science* 256 (2010) pp 3592 – 3597

[32] Y. Y. Peng, T. E. Hsieh, C. H. Hsu. White-light emitting ZnO–SiO_2 nanocomposite thin films prepared by the target-attached sputtering method. *Nanotechnology* 17 (2006) pp 174 – 180

[33] F. W. H. Kruger, W. J. McGill. A DSC study of curative interactions. I. The interaction of ZnO, sulfur, and stearic acid. *J. Appl. Polym. Sci.* 42 (1991) pp 2643 – 2649,

[34] F. W. H. Kruger, W. J. McGill. A DSC study of curative interactions. II. The interaction of 2,2′-dibenzothiazole with ZnO, sulfur, and stearic acid. *J. Appl. Polym. Sci.* 42 (1991) pp 2651 – 2659

[35] M. A. Mesubi. An infrared study of zinc, cadmium, and lead salts of some fatty acids. *J. Mol. Struct.* 81 (1982) pp 61 – 71

[36] J. Špačková, C. Fabra, S. Mittelette, E. Gaillard, C.-H. Chen, G. Cazals, A. Lebrun, S. Sene, D. Berthomieu, K. Chen. Unveiling the Structure and Reactivity of Fatty-Acid Based (Nano)Materials Thanks to Efficient and Scalable ^{17}O and ^{18}O-Isotopic Labeling Schemes. *J. Am. Chem. Soc.* 142 (2020) pp 21068 – 21081

[37] J. De Roo, E. A. Baquero, Y. Coppel, K. De Keukeleere, I. Van Driessche, C. Nayral, Z. Hens, F. Delpech. Insights into the Ligand Shell, Coordination Mode, and Reactivity of Carboxylic Acid Capped Metal Oxide Nanocrystals. *ChemPlusChem* 81 (2016) pp 1216 – 1223

[38] B. H. Ye, X. Y. Li, I. D. Williams, X. M. Chen. Synthesis and structural characterization of di- and tetranuclear zinc complexes with phenolate and carboxylate bridges. Correlations between 13C NMR chemical shifts and carboxylate binding modes. *Inorganic Chemistry* 41 (2002) pp 6426 –6431

[39] J. Catalano; Y. Yao, A. Murphy, N. Zumbulyadis, S. A. Centeno, C. Dybowski. Nuclear Magnetic Resonance Spectra and 207Pb Chemical-Shift Tensors of Lead Carboxylates Relevant to Soap Formation in Oil Paintings. *Appl. Spectrosc*. 68 (2014) pp 280 – 286

[40] A. Patra, T. K. Sen, R. Bhattacharyya, S. K. Mandal, M. Bera. Diversity of carboxylate binding in a new tetranuclear zinc cluster: correlation between spectroscopic investigations and carboxylate binding modes. *RSC Adv.* 2 (2012) pp 1774 – 1777

Electronic Supporting Information for

Studying stearic acid interaction with ZnO/SiO_2 nanoparticles with tailored morphology and surface features: a benchmark for better designing efficient ZnO-based curing activators

Silvia Mostoni [a], Paola Milana [a], Massimiliano D'Arienzo [a], Sandra Dirè [b], Emanuela Callone [b], Cinzia Cepek [c], Silvia Rubini [c], Aysha Farooq [c], Carmen Canevali [a], Barbara Di Credico [a] and Roberto Scotti [a,d]*

[a] Department of Materials Science, INSTM, University of Milano-Bicocca, Via R. Cozzi 55, 20125 Milano, Italy;

[b] Department of Industrial Engineering (DII), University of Trento, Via Sommarive 9, 38123, Trento, Italy;

[c] Istituto Officina dei Materiali-CNR Laboratorio TASC, Strada Statale 14, km 163.4, I-34012 Trieste, Italy

[d] Istituto di Fotonica e Nanotecnologie-CNR, via alla Cascata, 56/C, 38100, Povo, Trento, Italy

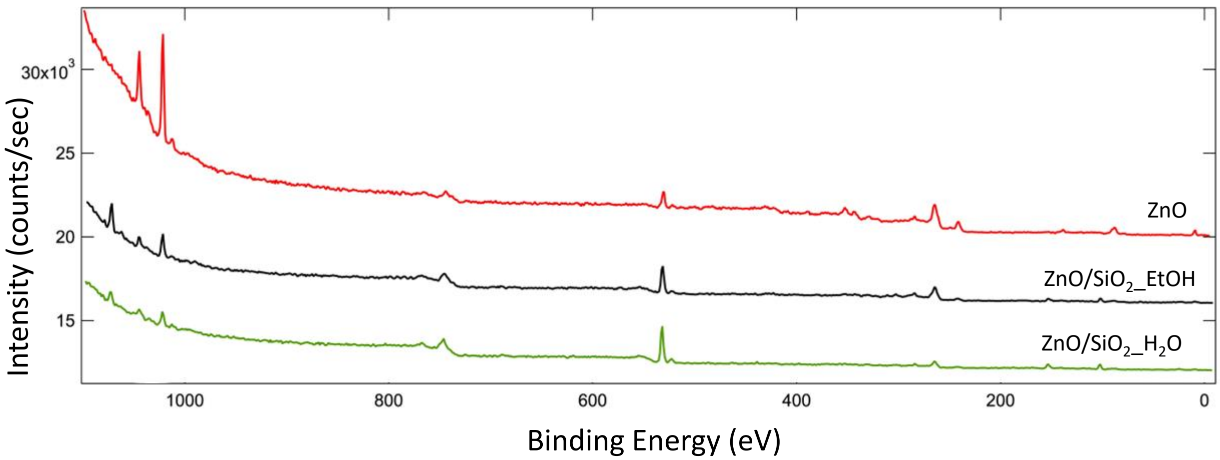

Figure S1. XPS wide survey spectra of pure ZnO (black line), ZnO/SiO_2_EtOH (red line) and ZnO/SiO_2_H_2O NPs (green line).

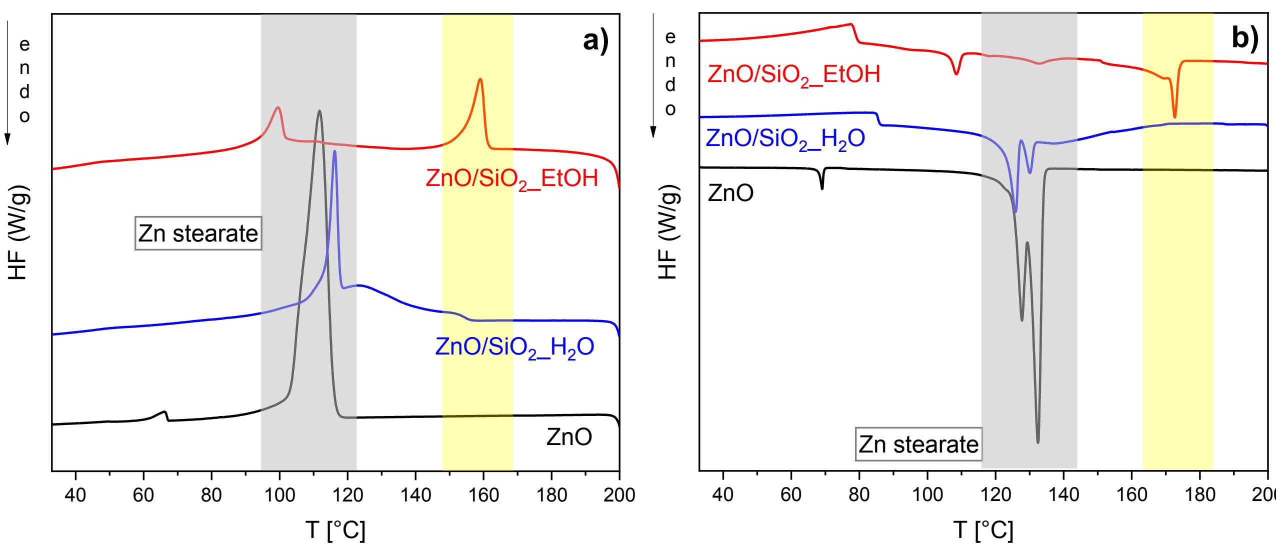

Figure S2. DSC curves of ZnO and ZnO/SiO_2 samples mixed with SA registered a) during the cooling ramp (monitored from 200 to 30 °C) and b) during the second heating ramp (from 30 to 200°C).

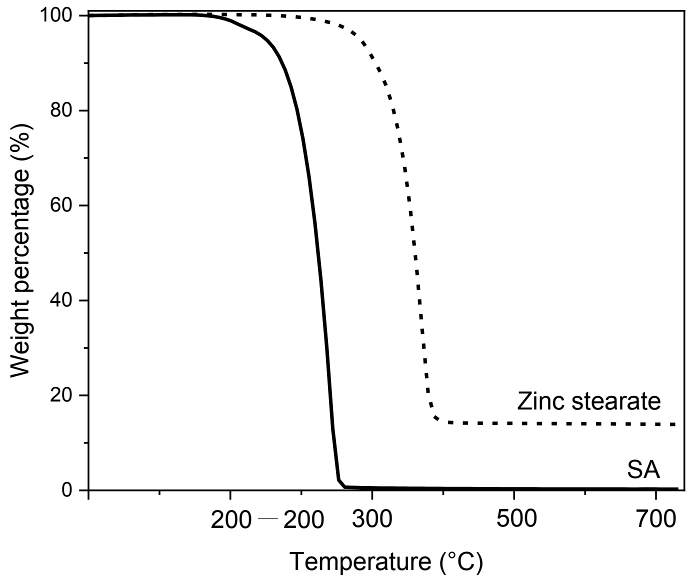

Figure S3. Thermal degradation profiles of zinc stearate (dashed line) and SA (bold line).